

P9.5 Multiple-Doppler Observations of a Nontornadic Supercell on 23 May 2002 Using Ground-Based Mobile Radars

JEFFREY FRAME*, PAUL MARKOWSKI, AND YVETTE RICHARDSON

Department of Meteorology, Pennsylvania State University, University Park, PA

JOSHUA WURMAN

Center for Severe Weather Research, Boulder, CO

1. Introduction

Two Doppler on Wheels (DOW) radars (Wurman et al. 1997) and the Greek X-Pol radar (Wurman 2001) intercepted a nontornadic supercell near Gage, Oklahoma, on 23 May 2002 during the International H₂O Project (IHOP; Weckwerth et al. 2004). The storm was initiated along a slow-moving cold front over the Texas Panhandle, and it was already supercellular when multiple-Doppler data collection began at 0000 UTC 24 May. A map of the deployment is provided in Fig. 1.

These data are of interest because they span a region far from the mesocyclone and updraft of the supercell. The region of the storm in close proximity to the mesocyclone tends to be the focus of most Doppler radar studies of supercells for rather obvious reasons. Initially, we had hoped to perform a wind synthesis over a broad region, both within the precipitation region and over much of the environmental inflow ahead of the storm. The clear-air echoes, however, were too weak and shallow, and there was not enough overlap between the clear-air returns from the various radars, to allow such a synthesis to be completed.

Ground-based, mobile Doppler radar observations, especially dual-Doppler, within the forward-flank downdraft have been limited, less frequent than mobile Doppler radar observations of tornadoes themselves. Yet, the forward flank is believed to be important dynamically (e.g., Klemp and Rotunno 1983; Rotunno and Klemp 1985). Herein, we document the forward flank of one nontornadic storm and present what may be some surprising results.

2. Data and methodology

Data from the three Doppler radars (DOW2, DOW3, and XPOL) were mapped to a Cartesian grid using a one-pass Barnes analysis (Barnes 1964). The Cartesian grid dimensions are $60 \times 60 \times 2$ km, with horizontal and vertical grid spacings of 400 m and 200 m, respectively. A smoothing parameter of $\kappa = 0.69 \text{ km}^2$ was used, and data beyond 1.8 km from a grid point did not contribute to the analysis at that grid point. An advective correction was incorporated into the analysis to compensate for the motion of the storm during the time required to complete a volume scan (approximately 120 s). The

extrapolation of data into data voids was not permitted during the objective analysis, which resulted in qualitatively better kinematic fields in the three-dimensional wind syntheses. The three-dimensional wind syntheses were constructed following Gamache (1997). This variational method minimizes a cost function that is formulated by considering the radial velocity projections from each radar, mass continuity, a lower boundary condition, and a filter that suppresses noise. More information about this method can be found in Gamache (1997).

3. Observations

When multiple-Doppler observations began at 0000 UTC 24 May 2002, the forward flank of the storm had a classic supercellular appearance (e.g., a “v”-shaped echo and a large reflectivity gradient along its right or southern flank; Fig. 2a). The storm began to weaken after 0000 UTC, such that by 0016 UTC, most of the classic supercellular structure was gone (Fig. 2b). By 0030 UTC (Fig. 2c), only a small echo core greater than 40 dBZ remained, and the storm had almost completely dissipated by 0100 UTC (not shown).

Throughout the analysis period, southeasterly storm-relative (s-r) winds were present at low-levels within the forward flank. The main updraft area and attendant mesocyclone are too far removed from one of the radars (DOW3) and the angles between the beams of the other two (DOW2 and XPOL) are too small in this region of the storm to produce a meaningful analysis of the updraft or mesocyclone (Fig. 1). For the above reasons, we will focus the remainder of our analysis on the forward flank of the storm while the supercell is mature, or close to 0000 UTC.

The steady southeasterly s-r flow within the forward flank suggests that, in this case, air parcels along and near the forward-flank gust front do not move toward the primary updraft (Fig. 2), as has been found in previous modeling studies (Klemp and Rotunno 1983; Rotunno and Klemp 1985). Seven trajectories were computed between 0000 UTC and 0010 UTC, all originating at 800 m above ground level (AGL) near the forward flank of the storm (Fig. 3a). The zonal separation between the trajectories was 5 km, while the meridional separation was allowed to vary depending on the shape of the echo, but is generally on the order of 3 km. Each trajectory depicts air parcels near the forward-flank baroclinic zone moving northwestward into the echo core by 0010 UTC, which is consistent with the s-r wind analysis presented above. It would have been desir-

*Corresponding author address: Jeffrey Frame, Department of Meteorology, Pennsylvania State University, 503 Walker Building, University Park, PA 16802; e-mail: jwf155@psu.edu

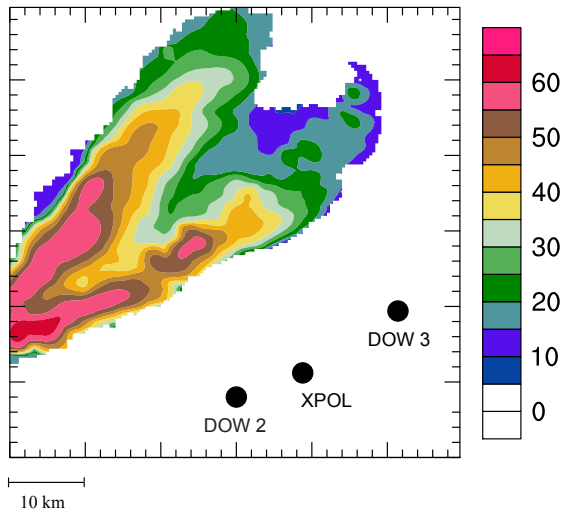


FIG. 1. XPOL radar reflectivity at 600 m AGL and the positions of the three mobile Doppler radars throughout the deployment. Equivalent reflectivity color scale (dBZ_e) is as indicated.

able to calculate trajectories originating even lower than 800 m AGL, but the parcels rapidly descended below the radar horizon owing to a downdraft located on the right flank of the storm (Fig. 3b). Even with an initial elevation of 800 m, some of the parcels still descended into a data void before the 10-minute trajectory calculation could be completed (Fig. 3a). Also note that no effort was made to extrapolate the trajectories into regions with missing data; a trajectory was terminated when it entered a region with no data.

There is also a slight indication of upward motion along what is likely the forward-flank gust front near the right flank of the main echo body (Fig. 3b), but this feature is located on the border of the region containing multiple-Doppler data, so its veracity is questionable.

A band of enhanced vertical vorticity (Fig. 3c) is located just behind the area of negative vertical velocities discussed above. This band moves northwestward in a *s-r* sense with time, as can be seen by the slight bend in the *s-r* wind vectors near the major axis of the radar echo at later times (Figs. 2b and 2c).

The low-level horizontal vorticity field in this case also differs from the conceptual model of a supercell thunderstorm put forth by Klemp (1987). In that model, the low-level vortex lines are oriented parallel to the forward-flank reflectivity gradient in the inflow south of the storm, then become oriented normal to the reflectivity gradient as they encounter it, such that they become directed toward the primary updraft of the storm. In this case, the low-level horizontal vorticity vector is oriented normal to the reflectivity gradient, but is directed *away* from the storm's main updraft region (Fig. 4). Also note that in that conceptual model, the reflectivity gradient and the horizontal buoyancy gradient are approximately parallel. A buoyancy retrieval for this case, done using the technique of Hane and Ray (1985), reveals that the horizontal buoyancy gradient is rather weak (generally around 0.1 K km^{-1} within most of the forward flank), and that there is likely not a large mass of cold air beneath the forward flank of this thunderstorm (Fig. 3d).

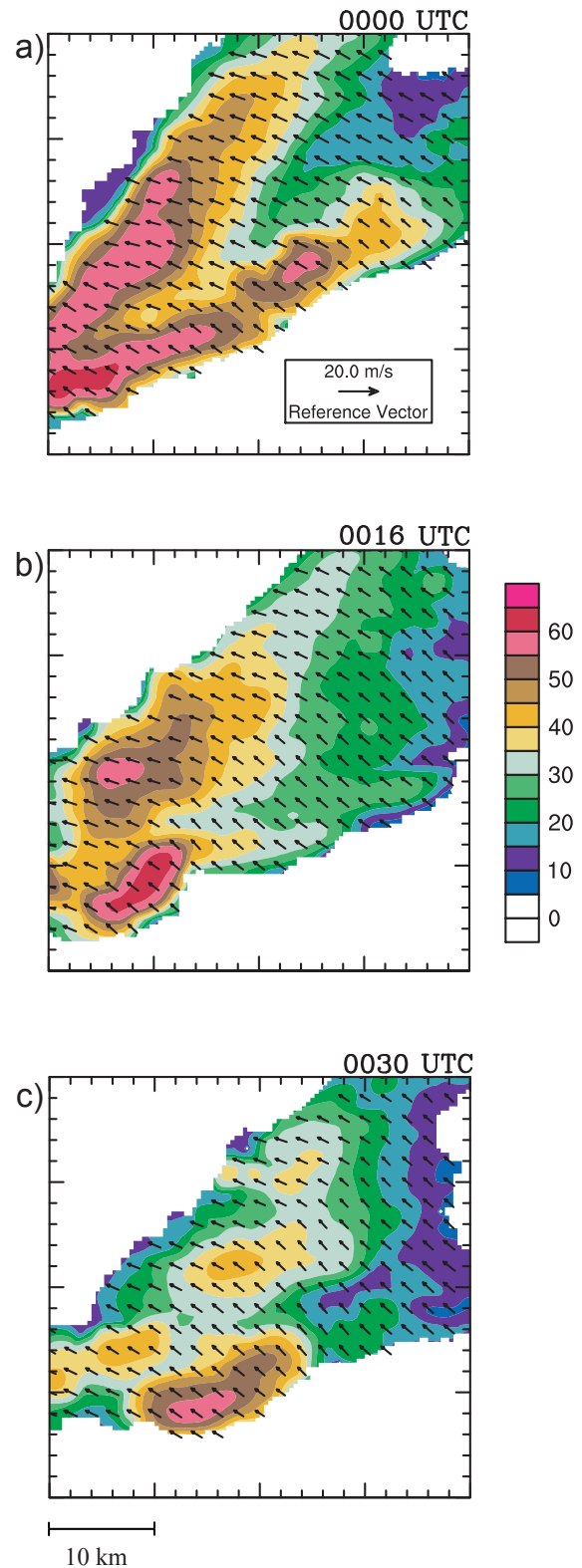


FIG. 2. XPOL radar reflectivity and storm-relative wind vectors analyzed at 600 m AGL for (a) 0000 UTC 24 May 2002, (b) 0016 UTC, and (c) 0030 UTC. Reflectivity color scale is as indicated.

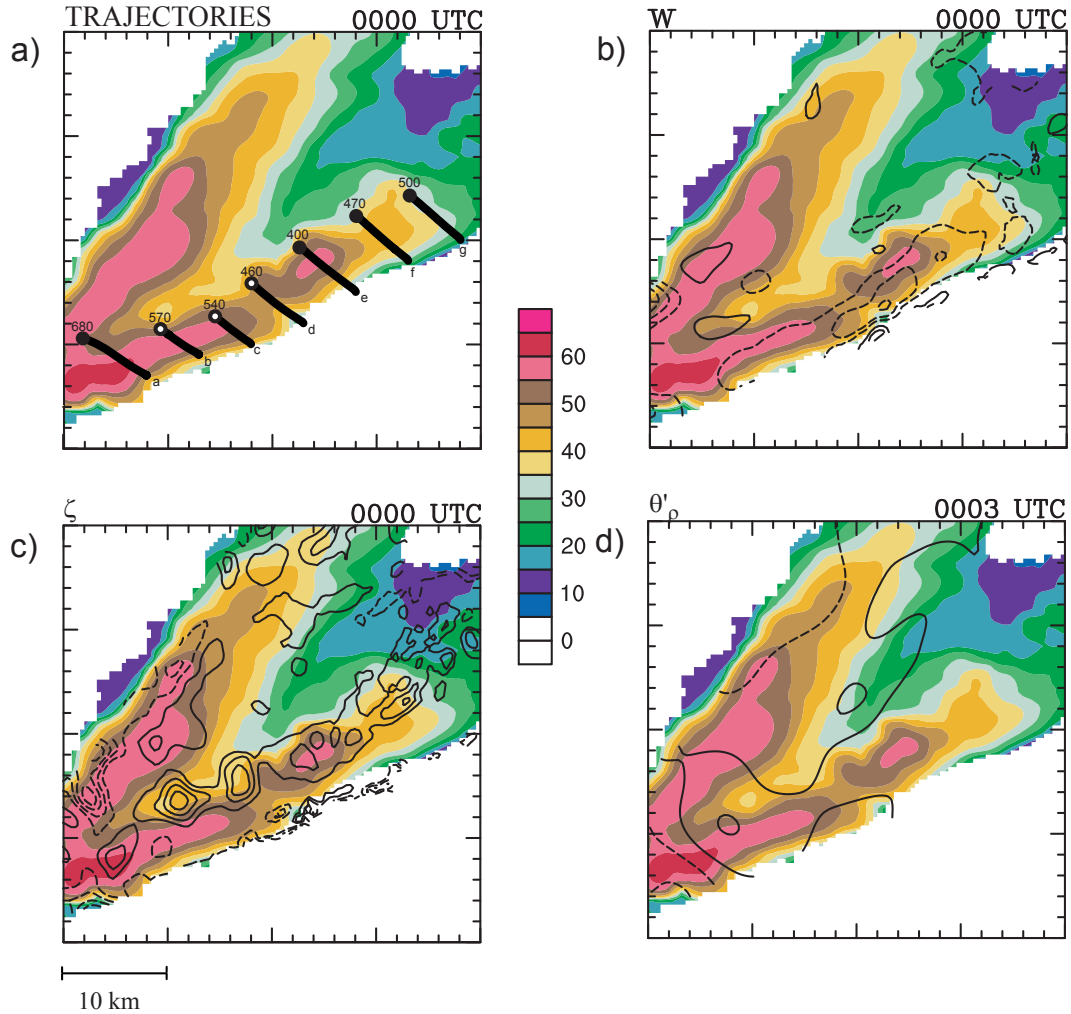


FIG. 3. XPOL radar reflectivity at 600 m AGL at 0000 UTC overlaid with (a) s-r trajectories, (b) 600 m vertical velocity, contoured every 0.5 m s^{-1} , (c) 600 m vertical vorticity, contoured every $0.5 \times 10^{-3} \text{ s}^{-1}$, and (d) 600 m θ'_p , contoured every 1.0 K . Reflectivity color scale is as indicated, and in (b) and (c), the zero contour has been omitted for clarity. Negative contours are dashed in all of the panels. A white circle at the end of a trajectory indicates that the trajectory was terminated early because it encountered missing data, whereas a filled circle indicates a full 10 minute calculation. The elevation of each trajectory at the end of each calculation is also given. Note that θ'_p does not have a unique solution; the sign does not necessarily imply an excess or a deficit with respect to the ambient environment.

It is possible, however, that all of the multiple-Doppler data are within the forward-flank outflow, so the buoyancy gradient along the forward-flank gust front may not be within the multiple-Doppler domain. A comparison between the s-r winds and trajectories (Figs. 2a and 3a) and the horizontal vorticity vector (Fig. 4c) also reveals that the horizontal vorticity in the right-forward flank of the storm is almost purely crosswise. Thus, the horizontal vorticity vector is not oriented favorably to be tilted by the storm's updraft and augment its low-level rotation. It is also possible that the environmental wind and horizontal vorticity fields are influencing the wind and horizontal vorticity fields within the storm.

The horizontal vorticity vector points northeastward south of the weak echo notch, and northwestward north of this notch (Figs. 4a and 4b). This reorientation of the horizontal vorticity vector is also coincident with a slight wind shift (Fig. 2), and maxima in the w and ζ fields (Figs. 3b and 3c). This feature

is rather curious, and is not present in conceptual models, but one cannot help but wonder if this structure is fairly common, because such reflectivity structures are often observed in supercells.

It is clear from the direction of the horizontal vorticity vector that ξ , the x -component of horizontal vorticity, is positive within the southern half of the forward-flank echo (Fig. 4c), whereas one would expect it to be negative based on the conceptual model of a supercell. Given that $\xi = \partial w / \partial y - \partial v / \partial z$, and noting that horizontal variations in w are small at low-levels (Fig. 3b), then the vertical shear of the meridional wind, v , should be responsible for the magnitude and sign of ξ . An analysis of v at 400 and 800 m AGL within the forward flank reveals that $\partial v / \partial z$ is negative within the right portion of the forward flank, and positive within the left portion (Fig. 4a and 4b). This results in $\xi > 0$ on the right flank and $\xi < 0$ on the left flank.

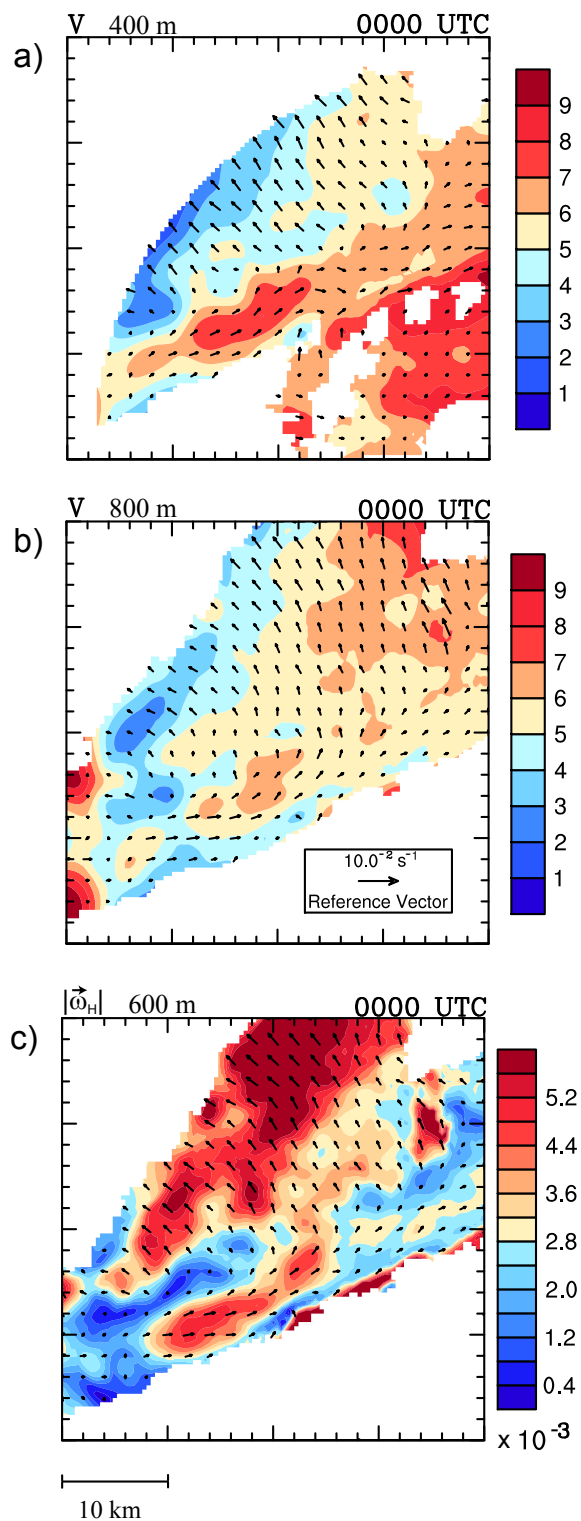


FIG. 4. Meridional wind component (shaded) and horizontal vorticity vector for 0000 UTC at (a) 400 m AGL, and (b) 800 m AGL. (c) Horizontal vorticity (vector; magnitude shaded) at 0000 UTC at 600 m AGL.

4. Conclusions

The multiple-Doppler observations presented herein allow us to investigate the kinematics within the forward flank of a supercell thunderstorm. This analysis indicates that air parcels within the forward-flank baroclinic zone, at least in this case, do not flow into the updraft, which is in contrast with most accepted conceptual models of supercell thunderstorms. The horizontal vorticity vector within this region is also oriented roughly 180 degrees from that which would be expected from most conceptual models. It is possible, however, that both the low-level wind and vorticity fields more closely matched the conceptual models outside the multiple-Doppler domain or at an earlier stage in the storm's evolution, before the onset of multiple-Doppler observations.

Nonetheless, this case study highlights the need for more fine-scale observations within all regions of supercell thunderstorms, not only the areas around the rear-flank downdraft and mesocyclone. Ideally, such a project would entail not only multiple Doppler radars, but also mobile probes capable of measuring the thermodynamic variables around and within the storm. It is our hope that such a project comes to fruition in the near future.

Acknowledgments. We are grateful to all of the IHOP volunteers (too numerous to mention) who helped with the data collection, and to Marios Anagnostou and Manos Anagnostou for providing the XPOL data. We also wish to thank John Gamache for sharing his variational wind synthesis technique and code, David Dowell and Nettie Arnott for sharing some of their code, and Jim Marquis and Brian Monahan for their assistance throughout this project. Support from NSF grant ATM-0437512 also is acknowledged.

REFERENCES

- Barnes, S. L., 1964: A technique for maximizing details in numerical weather map analysis. *J. Appl. Meteor.*, **3**, 396–409.
- Gamache, J. F., 1997: Evaluation of a fully three-dimensional variational Doppler analysis technique. Preprints, *28th Conf. on Radar Meteorology*, Austin, TX, Amer. Meteor. Soc., 422–423.
- Hane, C. E. and P. S. Ray, 1985: Pressure and buoyancy fields derived from Doppler radar data in a tornadic thunderstorm. *J. Atmos. Sci.*, **42**, 18–35.
- Klemp, J. B., 1987: Dynamics of tornadic thunderstorms. *Annu. Rev. Fluid Mech.*, **19**, 369–402.
- Klemp, J. B. and R. Rotunno, 1983: A study of the tornadic region within a supercell thunderstorm. *J. Atmos. Sci.*, **40**, 359–377.
- Rotunno, R. and J. B. Klemp, 1985: On the rotation and propagation of simulated supercell thunderstorms. *J. Atmos. Sci.*, **42**, 271–292.
- Weckwerth, T. M., and Coauthors, 2004: An overview of the International H₂O Project (IHOP) and some preliminary highlights. *Bull. Amer. Meteor. Soc.*, **85**, 253–277.
- Wurman, J. M., 2001: The DOW Multiple-Doppler Network. Preprints, *30th International Conf. on Radar Meteorology*, Munich, Germany, Amer. Meteor. Soc., 95–97.
- Wurman, J. M., J. M. Straka, E. N. Rasmussen, M. Randall, and A. Zahrai, 1997: Design and deployment of a portable, pencil-beam, pulsed, 3-cm Doppler radar. *J. Atmos. Oceanic Technol.*, **14**, 1502–1512.